EARTHQUAKE ENGINEERING AND STRUCTURAL DYNAMICS, VOL. 26, 931–949 (1997)

SPRING-DASHPOT-MASS MODELS FOR FOUNDATION VIBRATIONS

JOHN P. WOLF*

Institute of Hydraulics and Energy, Department of Civil Engineering, Swiss Federal Institute of Technology Lausanne, CH-1015 Lausanne, Switzerland

SUMMARY

The foundation on deformable soil, which, in general, radiates energy, can be represented in structural dynamics as a simple spring-dashpot-mass model with frequency-independent coefficients. For the two limiting cases of a site, the homogeneous half-space and the homogeneous layer fixed at its base, the coefficients are specified in tables for varying parameters such as ratios of dimensions and Poisson's ratio. Rigid foundations on the surface and with embedment are considered for all translational and rotational motions. In a practical analysis of soil–structure interaction this dynamic model of the foundation is coupled directly to that of the structure, whereby a standard dynamics program is used.

Earthquake Engng. Struct. Dyn., **26**, 931–949 (1997)

No. of Figures: 18. No. of Tables: 7. No. of References: 17.

KEY WORDS: dynamic stiffness; foundation vibration; soil–structure interaction; spring-dashpot-mass model

1. INTRODUCTION

1.1. Statement of problem

The fundamental objective of a dynamic *unbounded soil–structure-interaction* analysis is illustrated in Figure 1. A structure with finite dimensions is embedded in deformable soil of infinite dimensions. Often the structure–soil interface, called the foundation in the following, can be regarded as rigid. The time-dependent load can either act directly on the structure, arising for instance from rotating machines or be introduced into the dynamic system via incident waves as from earthquakes. The dynamic response of the structure interacting with the soil is to be determined.

The modelling of the structure, which can also exhibit non-linear behaviour, is well developed. The finite-element method is used, which with a finite number of degrees of freedom can be interpreted physically as consisting of generalised springs, dashpots and masses. Powerful and user-friendly computer programs for the dynamic analysis of structures are available. In contrast, difficulties exist in modelling the foundation on linear soil. Its deformability and the radiation of energy towards infinity must be considered. For large projects of critical facilities such as the seismic analysis of nuclear power plants, rigorous procedures based on three-dimensional elastodynamics as the boundary-element method or the consistent infinitesimal finite-element cell method are available. Due to the considerable manpower and computational effort required to apply these rigorous methods, it is difficult to perform the necessary parametric studies and to investigate alternative design schemes. They obscure physical insight and belong with their mathematical complexity more to the discipline of applied computational mechanics than to civil engineering.

For everyday practical *foundation-vibration analyses*, the majority, *simple physical models* can be used with a small number of degrees of freedom and a few springs, dashpots and masses whose frequency-independent

* Correspondence to: J. P. Wolf, Institute of Hydraulics and Energy, Department of Civil Engineering, Swiss Federal Institute of Technology Lausanne, CH-1015 Lausanne, Switzerland

CCC 0098–8847/97/090931–19$17·50

Received 8 August 1996
Revised 28 January 1997

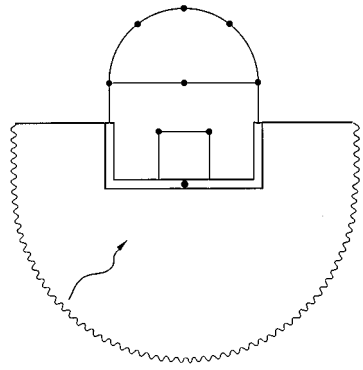

Figure 1. Objective of dynamic unbounded soil–structure interaction analysis

coefficients follow directly for the important cases from tables. The modelling of the foundation on deformable soil is thus performed in the same way as that of the structure. It is also possible to couple the models of the structure and of the soil and to perform a dynamic unbounded soil–structure-interaction analysis using a standard structural dynamics program directly in the time domain. This natural approach considers the sequence of developments from one time step to the next and also permits the structure to exhibit non-linear behaviour, which can only be analysed efficiently in the time domain.

1.2. Strength-of-materials approach to foundation dynamics

The spring-dashpot-mass models can be regarded as a first step towards developing a *strength-of-materials approach to foundation dynamics*, analogous to beam theory in structural analysis with a restricted deformation behaviour (plane sections remain plane). In this strength-of-materials theory for soil the three-dimensional homogeneous half-space is replaced by a one-dimensional truncated semi-infinite cone (rod, bar) as described in References 1 and 2. It is important to note that this truncated cone modelling a circular foundation on the surface of a homogeneous soil half-space corresponds exactly to a spring-dashpot system (and for the rotational degrees of freedom also to a mass moment of inertia with its own degree of freedom) as developed in the pioneering paper[3] and illustrated in Reference 4. A thorough discussion is found in References 5 and 6. The only approximation thus consists of replacing the half-space by a truncated cone model, which the engineer can comprehend physically. Such an approach with physical insight is better than a mathematical approximation, which could for instance consist of neglecting certain terms with higher derivatives in the differential equations of three-dimensional elastodynamics.

As next step, without changing the arrangement, the coefficients of the spring-dashpot-mass model can be determined applying curve fitting instead of using those of the truncated cone. This permits–for a certain frequency range–to minimize the deviation (defined as the sum of the squares) of the approximate solution of the spring-dashpot-mass model from the rigorous result of the boundary-element method, the consistent infinitesimal finite-element cell method or the analytical expression, when available, taken from the literature.

The simple models[7–9] used often in practice for a foundation on the surface of or embedded in a homogeneous soil half-space can be derived using this procedure. As a generalization, a systematic method has been developed[10] to construct spring-dashpot-mass models by placing the basic arrangement of the truncated cone in parallel. After the curve fitting leading to a rational function in frequency of the dynamic-stiffness coefficients, no further approximation is introduced. This permits foundations on the surface of or embedded in a homogeneous soil layer fixed at its base to be modelled.[11] The coefficients of the springs, dashpots and masses are listed in tables for all degrees of freedom for varying parameters such as ratios of dimensions and

Poisson's ratio. Material damping of the soil can be introduced directly in the algorithm of the spring-dashpot-mass model.[12]

Over the years, several authors have developed other spring-dashpot-mass models to represent a foundation on deformable soil. The results are only available for special cases. They are thus not listed in this hand-book type summary paper to be used directly by the practicing engineer for a broad class of every-day foundation vibration analyses.

In passing, it is worth mentioning that by using directly truncated cones, a strength-of-materials theory for most cases of foundation dynamics has been developed, covering surface and embedded foundations and piles, even in a layered half-space.

Methods which postulate a specific wave pattern in the horizontal plane with the corresponding displacements also belong to the strength-of-materials theory of foundations. This permits Green's function to calculate irregular surface foundations and dynamic-interaction factors to consider pile group effects to be determined.

The three types of *simple physical models*—the *truncated cones*, the *spring-dashpot-mass models* and the *methods with a prescribed wave pattern in the horizontal plane*—are examined in great detail in a book[13] published recently. Simple physically motivated derivations, many examples and practical applications are addressed. Use of these simple physical models leads to some loss of precision, but this is more than compensated for by their many advantages. The simple physical models provide *physical insight and conceptual clarity*, are *simple to apply* (in many cases on the back of the famous envelope), exhibit *sufficient generality* (shape of foundation, soil profile, embedment) and lead to *sufficient engineering accuracy*. They can thus be applied for everyday practical foundation-vibration analyses in a design office. In addition, the simple physical models can be used to check the results of rigorous methods such as the boundary-element procedure or the consistent infinitesimal finite-element cell method.

1.3. Accuracy

To demonstrate the obtainable accuracy, the vertical degree of freedom of a circular rigid massless disk of radius r_0 on the surface of a homogeneous layer fixed at its base of depth d and Poisson's ratio v is investigated (Figure 10). This is a very stringent test as this dynamic system is dispersive and exhibits a cutoff frequency. The following values are selected: $r_0 = d$ and $v = 1/3$. The spring-dashpot-mass model (Figure 11) has, besides the degree of freedom of the foundation u_0, also two internal degrees u_1 and u_2. Four springs, three dashpots and one mass are present with frequency-independent coefficients determined for vertical translation, $r_0/d = 1$ and $v = 1/3$ from Table VI. As the spring-dashpot-mass system is exact for statics and the limit of infinite frequency, only six coefficients are independent.

For harmonic excitation of frequency ω the dynamic-stiffness coefficient defined as the ratio of the amplitude of the applied load $P_0(a_0)$ to that the resulting displacement $u_0(a_0)$ is written as

$$S(a_0) = K[k(a_0) + \mathrm{i}a_0 c(a_0)] \tag{1}$$

with the dimensionless frequency $a_0 = \omega r_0/c_s$ (shear-wave velocity c_s). In this complex-variable notation K represents the static-stiffness coefficient, $k(a_0)$ the dimensionless spring coefficient and $c(a_0)$ the corresponding damping coefficient. From the comparison of $k(a_0)$ and $c(a_0)$ calculated with the spring-dashpot-mass model shown as a thick line in Figure 2 with the rigorous solution denoted as exact of elastocynamics[14] it follows that the agreement is good. In particular, the spring-dashpot-mass model can represent accurately the vanishing $c(a_0)$ below the cutoff frequency, where no radiation of energy occurs.

As an example of a dynamic analysis in the time domain the vertical displacement $u_0(t)$ is calculated caused by a load applied as a unit impulse at $t = 0$ (Figure 3). Again, the deviations from the exact solution are small. A very large number of comparisons of results determined using the simple physical models with rigorous solutions is described in Reference 13.

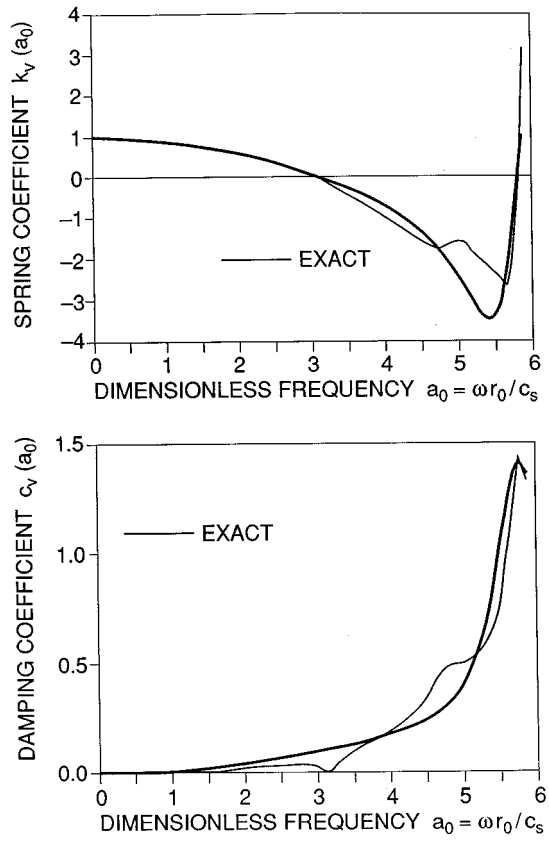

Figure 2. Vertical dynamic–stiffness coefficient of disk on surface of layer

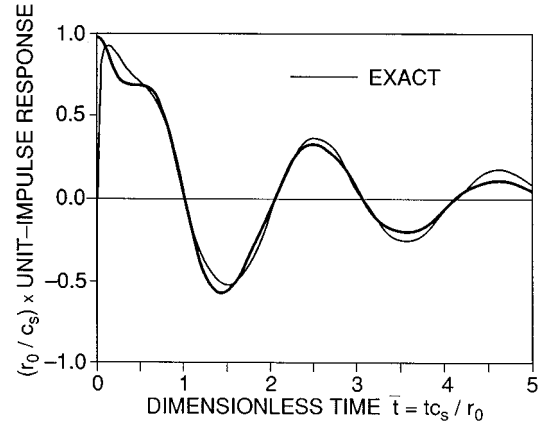

Figure 3. Vertical displacement caused by unit-impulse force acting on disk on surface of layer

1.4. Overview of tables with coefficients of spring-dashpot-mass models for dynamic-stiffness coefficients of foundations

In the following sections, the data required to construct the spring-dashpot-mass models of foundations for the two limiting cases of a site, the homogeneous half-space and the homogeneous layer fixed at its base, are presented. The spring-dashpot-mass models are also called lumped-parameter models. Massless rigid foundations on the surface of and embedded in the soil are addressed, varying the parameters extensively. The data listed in the tables consist, in general, of the dimensionless coefficients of the springs, dashpots and masses, the static-stiffness coefficients and eccentricities, if applicable. Some of the coefficients will be negative, but real. Springs, dashpots and masses with negative coefficients do not exist in reality. It is thus actually not possible to build this model mechanically; but to handle such as a model mathematically is, of course, no problem. Direct integration is recommended to solve the equations of motion. As already mentioned, the spring-dashpot-mass model of the foundation with a few internal degrees of freedom can be attached directly to the node at the base of the dynamic model of the structure, and the coupled dynamic system can be analysed directly with a standard structural dynamics program. This procedure permits consideration of dynamic unbounded soil–structure interaction with a computational effort which is hardly larger than when the structure only is analysed.

In the following, only those aspects required for a practical dynamic analysis are addressed. As an example, a hammer foundation with non-linear behaviour is calculated. The derivations, assumptions and further examples are described in the cited references and extensively in the book.[13] It is assumed that the dynamic loads act directly on the structure. For earthquakes and other excitations introduced into the dynamic system via the soil, the spring-dashpot-mass models can also be used. In this case the so-called effective foundation input motion is enforced in a first step at the foundation (base) node (where the structure will later be connected) of the spring-dashpot-mass model of the foundation, leading to the reaction forces. (The effective foundation input motion can also be determined using simple physical models, starting from the seismic free-field response). The reaction forces are then applied in a second step as an exterior load acting in the base node of the coupled dynamic system, yielding the dynamic response. This procedure is described in Section 6.5 of Reference 13.

As an example of an extension, spring-dashpot-mass models can also be constructed to determine the dynamic soil pressure acting on a vertical rigid wall retaining a semi-infinite uniform soil layer for horizontal seismic excitation.

2. DISK ON SURFACE HALF-SPACE

Three possibilities to model a rigid massless disk on the surface of a homogeneous half-space (Figure 4) for all components of motion (horizontal, vertical, rocking, torsional) are discussed. They differ in the assumptions, number of degrees of freedom and thus computational effort and in the accuracy.

2.1. Truncated cone model

For all components of motion a rigid massless foundation with area A_0 and (polar) moment of inertia I_0 on the surface of a homogeneous half-space with Poisson's ratio ν, mass density ρ, shear-wave velocity c_s, dilatational-wave velocity c_p can be modelled as a truncated cone (Figure 5a and Table I) of equivalent radius r_0, apex height z_0 and wave velocity c ($c_s = \sqrt{G/\rho}$, $c_p = \sqrt{E_c/\rho}$ with shear modulus G and constrained modulus $E_c = G2(1-\nu)/(1-2\nu)$). The aspect ratio z_0/r_0 is a function of ν. For the horizontal and torsional motions leading to shear strains the wave velocity c equals c_s. For the vertical and rocking motions resulting in axial strains c equals c_p for $\nu \leqslant 1/3$ and $c = 2c_s$ for $1/3 < \nu \leqslant 1/2$. The translational cone for the displacement u_0 and the force P_0 is dynamically equivalent to the spring-dasphot model (Figure 5(b)). The rotational cone for the rotation ϑ_0 and the moment M_0 corresponds exactly to the spring-dashpot-mass model with one internal degree of freedom ϑ_1 (Figure 5(c)), of which two possibilities are shown. In the model

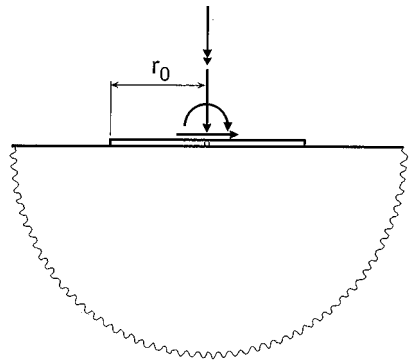

Figure 4. Rigid disk on homogeneous half-space

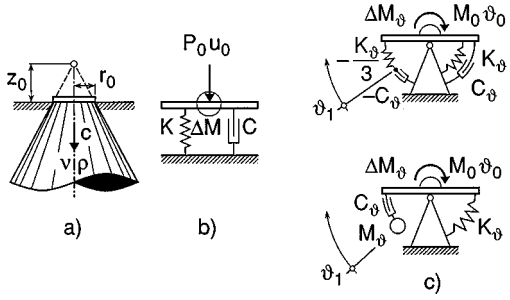

Figure 5. Cone model and equivalent spring-dashpot-mass model: (a) truncated semi-infinite cone; (b) spring-dashpot-mass model for translation; (c) spring-dashpot-mass models for rotation

without the mass moment of inertia M_ϑ two of the coefficients are negative. All coefficients (Table I) of the spring-dashpot-mass models, denoted as discrete-element models, are frequency independent. For the vertical and rocking motions for $1/3 < \nu \leqslant 1/2$ an additional trapped mass ΔM and mass moment of inertia ΔM_ϑ are present which are assigned to the disk's node.

This spring-dashpot-mass model corresponds exactly (without any curve fitting) to the physical assumption of replacing the three-dimensional halfspace below the disk by a one-dimensional truncated semi-infinite cone.

2.2. *Spring-dashpot-mass model without internal degree of freedom*

This simple arrangement corresponding to Figure 5(b) is shown for the translational and rotational motions in Figures 6(a) and 6(b) with the data listed in Table II. Besides a spring with the static-stiffness coefficient K, a dashpot C and a mass M (mass moment of inertia for rotation) are present with the coefficients

$$C = \frac{r_0}{c_s}\gamma K, \qquad M = \frac{r_0^2}{c_s^2}\mu K \tag{2a,b}$$

Note that γ and μ for the rotational motions are also a function of the mass moment of inertia m of the structure (that part which rotates as a rigid body in phase with the foundation).

Table I. Geometry and wave velocity of cone model and coefficients of spring-dashpot-mass model of Figure 5 for disk on half-space

Motion	Horizontal	Vertical	Rocking	Torsional
Equivalent radius r_0	$\sqrt{\frac{A_0}{\pi}}$	$\sqrt{\frac{A_0}{\pi}}$	$\sqrt[4]{\frac{4I_0}{\pi}}$	$\sqrt[4]{\frac{2I_0}{\pi}}$
Aspect ratio $\frac{z_0}{r_0}$	$\frac{\pi}{8}(2-\nu)$	$\frac{\pi}{4}(1-\nu)\left(\frac{c}{c_s}\right)^2$	$\frac{9\pi}{32}(1-\nu)\left(\frac{c}{c_s}\right)^2$	$\frac{9\pi}{32}$
Poisson's ratio ν	All ν	$\leqslant\frac{1}{3}$ $\frac{1}{3}<\nu<\frac{1}{2}$	$\leqslant\frac{1}{3}$ $\frac{1}{3}<\nu\leqslant\frac{1}{2}$	All ν
Wave velocity c	c_s	c_p $2c_s$	c_p $2c_s$	c_s
Trapped mass ΔM ΔM_ϑ	0	0 $2{\cdot}4\left(\nu-\frac{1}{3}\right)\rho A_0 r_0$	0 $1{\cdot}2\left(\nu-\frac{1}{3}\right)\rho I_0 r_0$	0
Discrete-element model	$K=\rho c^2 A_0/z_0$ $C=\rho c A_0$		$K_\vartheta=3\rho c^2 I_0/z_0$ $C_\vartheta=\rho c I_0$ $M_\vartheta=\rho I_0 z_0$	

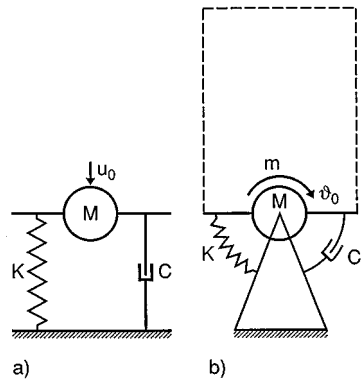

Figure 6. Spring-dashpot-mass model without internal degree of freedom for: (a) translation; (b) rotation

In this spring-dashpot-mass model only the degrees of freedom of the foundation node are present. The coefficients γ and μ are selected to reproduce as closely as possible the actual response of the coupled dynamic system (including the structure regarded as a rigid block with mass connected to the disk) in the low- and medium-frequency ranges.

2.3. Spring-dashpot-mass model with internal degree of freedom

This arrangement corresponding to the lower part of Figure 5(c) is shown for the motion u_0 and force P_0 in Figure 7 with the data listed in Table III. Besides a spring with the static-stiffness coefficient K and a dashpot C_0, which connect the disk with its own mass M_0 (mass moment of inertia for rotation) to a rigid support, an

Table II. Static-stiffness and dimensionless coefficients of spring-dashpot-mass model of Figure 6 for disk on half-space

	Static stiffness K	Dimensionless coefficients of Dashpot γ	Mass μ
Horizontal	$\frac{8Gr_0}{2-\nu}$	0·58	0·095
Vertical	$\frac{4Gr_0}{1-\nu}$	0·85	0·27
Rocking	$\frac{8Gr_0^3}{3(1-\nu)}$	$\frac{0{\cdot}3}{1+\frac{3(1-\nu)m}{8r_0^5\rho}}$	0·24
Torsional	$\frac{16Gr_0^3}{3}$	$\frac{0{\cdot}433}{1+\frac{2m}{r_0^5\rho}}\sqrt{\frac{m}{r_0^5\rho}}$	0·045

Table III. Static-stiffness and dimensionless coefficients of spring-dashpot-mass model of Figure 7 for disk on half-space

	Static stiffness K	Dimensionless coefficients of Dashpots γ_0	Dashpots γ_1		Masses μ_0	Masses μ_1
Horizontal	$\frac{8Gr_0}{2-\nu}$	0·78–0·4ν	—		—	—
Vertical	$\frac{4Gr_0}{1-\nu}$	0·8	0·34–4·3ν^4	$\nu<\frac{1}{3}$	0	0·4–4ν^4
				$\nu>\frac{1}{3}$	$0{\cdot}9\left(\nu-\frac{1}{3}\right)$	
Rocking	$\frac{8Gr_0^3}{3(1-\nu)}$	—	0·42–0·3ν^2	$\nu<\frac{1}{3}$	0	0·34–0·2ν^2
				$\nu>\frac{1}{3}$	$0{\cdot}16\left(\nu-\frac{1}{3}\right)$	
Torsional	$\frac{16Gr_0^3}{3}$	0·017	0·291		—	0·171

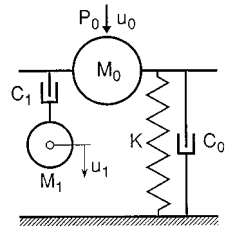

Figure 7. Spring-dashpot-mass model with internal degree of freedom

internal degree of freedom u_1 with its own mass M_1 (mass moment of inertia for rotation) is introduced. The latter is attached by a dashpot C_1 to the disk. The coefficients are calculated as

$$C_0 = \frac{r_0}{c_s}\gamma_0 K, \qquad C_1 = \frac{r_0}{c_s}\gamma_1 K \tag{3a,b}$$

$$M_0 = \frac{r_0^2}{c_s^2}\mu_0 K, \qquad M_1 = \frac{r_0^2}{c_s^2}\mu_1 K \tag{3c,d}$$

In this spring-dashpot-mass model the dimensionless coefficients $\gamma_0, \gamma_1, \mu_0, \mu_1$ are derived with curve fitting using the discrete values for various v specified in Reference 15 for the translational and rocking motions. This model is thus more accurate than those described in Tables I and II. It is of interest to perform a comparison with the spring-dashpot-mass model of the cone without any curve fitting. Equating the coefficients of the discrete-element model of Table I to the corresponding values in equation (3) leads to the dimensionless coefficients $\gamma_0, \gamma_1, \mu_0, \mu_1$ which are listed in Table IV.

3. CYLINDER EMBEDDED IN HALF-SPACE

A rigid massless cylinder embedded with depth e in a homogeneous half-space is addressed (Figure 8). For the vertical and torsional motions the spring-dashpot-mass model with one internal degree of freedom of Figure 7 with $M_0 = 0$ is constructed using the data of Table V and equation (3) [9].

To represent the coupling of the horizontal motion u_0 with the force P_0 and the rocking motion ϑ_0 with the moment M_0 (Figure 9), the spring-dashpot model for the horizontal motion u_0 corresponding to Figure 5(b) is connected to the centre of the cylinder's base with the eccentricities

$$f_K = 0{\cdot}25e, \qquad f_C = 0{\cdot}32e + 0{\cdot}03e\left(\frac{e}{r_0}\right)^2 \tag{4a, b}$$

The spring K_h with the static-stiffness coefficient K and the dimensionless coefficient γ_0 of the dashpot are specified in Table V with

$$C_{0h} = \frac{r_0}{c_s}\gamma_0 K \tag{5}$$

For the rocking motion ϑ_0 the spring-dashpot-mass model with one internal degree of freedom of Figure 7 with $M_{0r} = 0$ is used. Note that the corresponding coefficients are defined with respect to K_r (and not K_{0r}), although K_{0r} is the coefficient of the spring which is attached to the rigid support:[13]

$$C_{0r} = \frac{r_0}{c_s}\gamma_0 K_r, \qquad C_{1r} = \frac{r_0}{c_s}\gamma_1 K_r, \qquad M_{1r} = \frac{r_0^2}{c_s^2}\mu_1 K_r \tag{6a–c}$$

Table IV. Static-stiffness and dimensionless coefficients of spring-dashpot-mass model of Figure 7 for disk on half-space represented as cone model of Figure 5

	Static stiffness K		Dimensionless coefficients of			
			Dashpots		Masses	
			γ_0	γ_1	μ_0	μ_1
Horizontal	$\frac{8Gr_0}{2-\nu}$		$0.79–0.39\nu$	—	—	—
		$\nu < \frac{1}{3}$	$1{\cdot}11\sqrt{(1-\nu)^3/(1-2\nu)}$		—	
Vertical	$\frac{4Gr_0}{1-\nu}$			—		—
		$\nu > \frac{1}{3}$	$1{\cdot}57(1-\nu)$		$1{\cdot}88\left(\nu-\frac{1}{3}\right)(1-\nu)$	
		$\nu < \frac{1}{3}$		$0{\cdot}42\sqrt{(1-\nu)^3/(1-2\nu)}$	—	$0{\cdot}52(1-\nu)^3/(1-2\nu)$
Rocking	$\frac{8Gr_0^3}{3(1-\nu)}$		—			
		$\nu > \frac{1}{3}$		$0{\cdot}59(1-\nu)$	$0{\cdot}35\left(\nu-\frac{1}{3}\right)(1-\nu)$	$1{\cdot}04(1-\nu)^2$
Torsional	$\frac{16Gr_0^3}{3}$		—	$0{\cdot}29$	—	$0{\cdot}26$

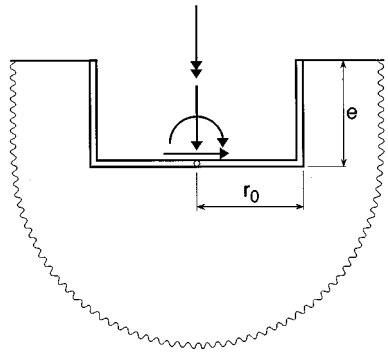

Figure 8. Rigid cylinder embedded in homogeneous half-space

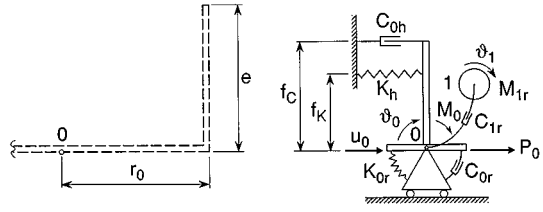

Figure 9. Spring-dashpot-mass model for cylinder embedded in half-space with coupling of horizontal and rocking motions

4. DISK ON SURFACE OF LAYER

A rigid massless disk on the surface of a homogeneous layer fixed at its base of depth d is discussed (Figure 10). For each motion u_0 with the force P_0 the spring-dashpot-mass model with two internal degrees of freedom u_1, u_2 shown in Figure 11 is ussed.[11] It consists of four springs K_i, three dashpots C_i and one mass M with the data specified in Table VI. The ratio of the radius to the depth r_0/d and Poisson's ratio v are varied. For the translational motions the coefficients equal (shear modulus G)

$$K_i = k_i G r_0, \quad i = 1, \ldots, 4 \tag{7a}$$

$$C_i = c_i G \frac{r_0^2}{c_s}, \quad i = 1, \ldots, 3 \tag{7b}$$

$$M = mG \frac{r_0^3}{c_s^2} \tag{7c}$$

For the rotational motions the right-hand side of equation (7) is multiplied by an additional r_0^2, e.g. $K_i = k_i G r_0^3$.

5. CYLINDER EMBEDDED IN LAYER

A rigid massless cylinder embedded in a homogeneous layer with Poisson's ratio $v = 1/3$ fixed at its base is discussed (Figure 12). The cylinder is laterally in contact with the neighbouring soil over the height e_c. The embedment ratio e/r_0 equals 1. For the vertical and torsional motions the spring-dashpot-mass model with

Table V. Static-stiffness and dimensionless coefficients of spring-dashpot-mass model of Figures 7 and 9 for cylinder embedded in half-space

		Dimensionless coefficients of		
		Dashpots		Mass
	Static stiffness K	γ_0	γ_1	μ_1
Horizontal	$\frac{8Gr_0}{2-\nu}\left(1+\frac{e}{r_0}\right)$	$0{\cdot}68+0{\cdot}57\sqrt{\frac{e}{r_0}}$	—	—
Vertical	$\frac{4Gr_0}{1-\nu}\left(1+0{\cdot}54\frac{e}{r_0}\right)$	$0{\cdot}80+0{\cdot}35\frac{e}{r_0}$	$0{\cdot}32$–$0{\cdot}01\left(\frac{e}{r_0}\right)^4$	0·38
Rocking	$K_r=\frac{8Gr_0^3}{3(1-\nu)}\left[1+2{\cdot}3\frac{e}{r_0}+0{\cdot}58\left(\frac{e}{r_0}\right)^3\right]$ $K_{0r}=K_r-\frac{Gr_0^3}{2(2-\nu)}\left(1+\frac{e}{r_0}\right)\left(\frac{e}{r_0}\right)^2$	$\left[\begin{array}{l}0{\cdot}15631\frac{e}{r_0}\\ -0{\cdot}08906\left(\frac{e}{r_0}\right)^2\\ -0{\cdot}00874\left(\frac{e}{r_0}\right)^3\end{array}\right]$	$0{\cdot}40+0{\cdot}03\left(\frac{e}{r_0}\right)^2$	$0{\cdot}33+0{\cdot}10\left(\frac{e}{r_0}\right)^2$
Torsional	$\frac{16Gr_0^3}{3}\left(1+2{\cdot}67\frac{e}{r_0}\right)$	—	$0{\cdot}29+0{\cdot}09\sqrt{\frac{e}{r_0}}$	$0{\cdot}20+0{\cdot}25\sqrt{\frac{e}{r_0}}$

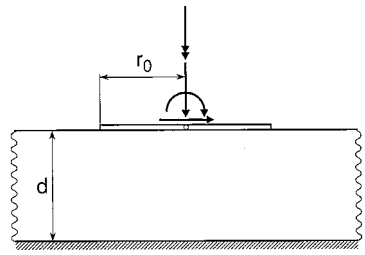

Figure 10. Rigid disk on homogeneous layer

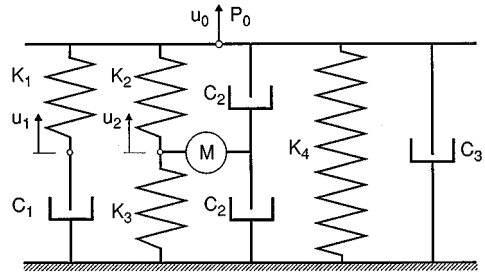

Figure 11. Spring-dashpot-mass model with two internal degrees of freedom

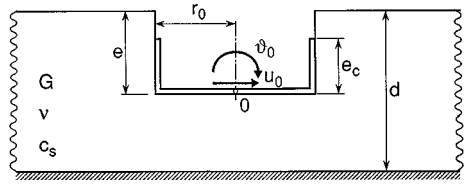

Figure 12. Rigid cylinder embedded in homogeneous layer

two internal degrees of freedom of Figure 11 is applied with the data listed in Table VII and using equation (7)[11]. The ratios of the radius to depth r_0/d and the contact ratio e_c/e are varied. To represent the coupling of the horizontal motion u_0 and the rocking motion ϑ_0, in addition to the models of these two motions, another spring-dashpot-mass model with the eccentricity equal to the embedded depth e is introduced. This spring-dashpot-mass model is denoted with the word Coupling in Figure 13 and Table VII.

6. HAMMER FOUNDATION WITH PARTIAL UPLIFT OF ANVIL

As a practical example of a non-linear unbounded soil–structure interaction analysis the vibration of a hammer foundation with an eccentrically mounted anvil is examined (Figure 14). The head impacts against the anvil which is a massive steel block. The anvil is supported by a viscoelastic suspension (pads) on a block of concrete which is embedded in a soil layer on rigid rock. As a tension-resistant connection is not provided for the pads, the anvil will partially uplift from the block when the dynamic stress (tension) exceeds the static stress (compression). A non-linear dynamic system thus occurs.

Table VI. Dimensionless coefficients of spring-dashpot-mass model of Figure 11 for disk on layer

Ratio of Radius to Depth r_0/d		Horizontal Poisson's ratio ν			Vertical Poisson's ratio ν			Rocking Poisson's ratio ν			Torsional
		0	1/3	0·45	0	1/3	0·45	0	1/3	0·45	
1·00	$k1$	−0·109636 E+02	−0·125658 E+02	−0·107091 E+02	−0·185216 E+02	−0·312572 E+02	−0·585650 E+02	−0·538137 E+01	−0·127100 E+02	−0·125057 E+02	−0·920277 E+01
	$k2$	−0·199616 E+02	−0·100143 E+02	−0·277613 E+02	−0·689058 E+02	+0·564651 E+01	+0·533868 E+02	−0·118019 E+02	−0·127000 E+01	−0·102097 E+02	−0·488643 E+01
	$k3$	−0·596293 E+03	−0·236814 E+03	−0·837270 E+03	−0·803915 E+04	−0·297570 E+04	−0·972054 E+05	−0·370561 E+03	−0·106411 E+03	−0·114401 E+05	−0·762034 E+02
	$k4$	+0·262006 E+02	+0·172890 E+02	+0·350886 E+02	+0·781698 E+02	+0·101028 E+02	−0·297301 E+02	+0·152717 E+02	+0·665102 E+01	+0·171002 E+02	+0·104850 E+02
	$c1$	−0·423955 E+01	−0·391585 E+01	−0·443420 E+01	−0·564579 E+01	−0·620122 E+01	−0·533597 E+01	−0·152562 E+01	−0·168764 E+01	−0·159579 E+01	−0·209847 E+01
	$c2$	−0·144980 E+02	−0·969345 E+01	−0·164981 E+02	−0·573623 E+02	−0·372925 E+02	−0·162817 E+03	−0·511671 E+01	−0·464871 E+01	−0·205038 E+02	−0·424955 E+01
	$c3$	+0·176380 E+02	+0·128349 E+02	+0·196381 E+02	+0·618023 E+02	+0·435725 E+02	+0·173237 E+03	+0·622671 E+01	+0·621871 E+01	+0·231038 E+02	+0·581955 E+01
	m	−0·444888 E+02	−0·177585 E+02	−0·804875 E+02	−0·355432 E+03	−0·896786 E+02	−0·759400 E+03	−0·136958 E+02	−0·294864 E+01	−0·748688 E+02	−0·501042 E+01
0·50	$k1$	−0·101741 E+02	−0·756096 E+01	−0·103098 E+02	−0·869429 E+01	−0·178038 E+02	−0·211241 E+02	−0·558202 E+01	−0·315920 E+01	−0·544861 E+01	−0·584813 E+01
	$k2$	−0·711128 E+01	+0·221036 E+01	+0·353643 E+00	−0·211429 E+02	+0·869558 E+01	+0·237930 E+02	−0·260867 E+01	+0·429528 E+00	+0·544528 E+01	+0·779373 E+00
	$k3$	−0·376551 E+02	−0·183990 E+02	−0·386290 E+02	−0·301954 E+03	−0·648930 E+02	−0·574768 E+04	−0·120186 E+02	−0·563639 E+00	−0·495529 E+02	−0·267204 E+01
	$k4$	+0·114651 E+02	+0·370791 E+01	+0·631911 E+01	+0·266455 E+02	+0·167960 E+00	−0·104560 E+02	+0·553603 E+01	+0·268680 E+01	−0·714571 E+00	+0·448746 E+01
	$c1$	−0·563146 E+01	−0·169515 E+01	−0·312323 E+01	−0·635435 E+01	−0·300736 E+01	−0·885920 E+01	−0·180105 E+01	−0·217449 E+00	−0·226588 E+01	−0·873265 E+00
	$c2$	−0·853329 E+01	−0·484337 E+01	−0·900332 E+01	−0·118278 E+02	−0·967485 E+01	−0·348879 E+02	−0·209944 E+01	−0·485884 E−01	−0·872006 E+00	−0·664093 E+00
	$c3$	+0·116733 E+02	+0·798337 E+01	+0·121433 E+02	+0·162678 E+02	+0·159548 E+02	+0·453079 E+02	+0·320944 E+01	+0·161859 E+01	+0·347201 E+01	+0·223409 E+01
	m	−0·125108 E+02	−0·142805 E+02	−0·222875 E+02	−0·438319 E+02	−0·104698 E+02	−0·156304 E+03	−0·166034 E+01	−0·550887 E−01	−0·105920 E+01	−0·758683 E+00
0·25	$k1$	−0·500393 E+01	−0·569922 E+01	−0·635602 E+01	−0·650348 E+01	−0·866267 E+01	−0·939217 E+01	−0·197103 E+01	−0·131566 E+01	−0·185845 E+01	−0·317223 E+01
	$k2$	+0·117908 E+01	+0·113372 E+01	+0·126563 E+01	+0·212837 E+01	+0·360033 E+01	+0·591506 E+01	−0·908392 E+00	−0·159178 E+01	+0·140842 E+01	−0·110204 E+02
	$k3$	−0·531658 E+01	−0·627809 E+01	−0·861155 E+01	−0·111486 E+02	−0·206851 E+02	−0·294639 E+02	+0·320667 E+00	+0·889908 E+00	−0·198123 E+01	−0·272014 E+02
	$k4$	+0·330564 E+01	+0·414181 E+01	+0·444955 E+01	+0·290606 E+01	+0·353509 E+01	+0·239510 E+01	+0·280516 E+01	+0·228996 E+01	+0·228257 E+00	+0·133791 E+02
	$c1$	−0·753687 E+00	−0·123420 E+01	−0·118324 E+01	−0·147587 E+01	−0·301652 E+01	−0·652332 E+01	−0·111891 E+01	−0·117566 E+01	−0·166191 E+01	−0·175255 E+01
	$c2$	−0·320391 E+01	−0·343160 E+01	−0·476257 E+01	−0·545496 E+01	−0·633133 E+01	−0·153512 E+01	−0·192001 E−01	−0·120420 E+00	−0·608065 E−01	−0·576183 E+00
	$c3$	+0·634391 E+01	+0·657160 E+01	+0·790257 E+01	+0·989496 E+01	+0·126113 E+02	+0·119551 E+02	+0·131920 E+01	+0·199042 E+01	+0·266081 E+01	+0·214618 E+01
	m	−0·197705 E+02	−0·277938 E+02	−0·353939 E+02	−0·202557 E+02	−0·262470 E+02	−0·217797 E+01	−0·496405 E−02	−0·234838 E−01	−0·166728 E−01	−0·408057 E+00
0·00	$k1$	−0·135004 E+02	−0·388471 E+01	−0·517262 E+01	−0·196175 E+01	−0·741830 E+01	−0·174454 E+02	−0·177328 E+01	−0·371794 E+01	−0·398695 E+01	−0·347454 E+01
	$k2$	−0·953646 E+01	−0·159784 E+02	+0·239313 E+00	−0·586095 E+00	+0·149859 E+01	+0·318590 E+01	−0·825315 E+01	−0·530262 E+01	+0·488296 E+01	+0·161189 E+00
	$k3$	−0·152937 E+02	−0·214052 E+02	−0·491200 E+01	+0·418313 E+00	−0·108130 E+02	−0·145871 E+03	−0·960129 E+00	−0·456729 E+01	−0·157465 E+02	−0·175021 E+00
	$k4$	+0·100318 E+02	+0·139890 E+02	+0·491843 E+01	+0·253876 E+01	+0·426031 E+01	+0·401297 E+01	+0·363207 E+01	+0·648378 E+01	−0·222776 E+01	+0·329151 E+01
	$c1$	−0·108173 E+01	−0·406936 E+00	−0·431719 E−01	−0·540639 E+00	−0·308148 E+00	−0·287195 E+01	−0·105544 E+01	−0·150532 E+01	−0·158356 E+01	−0·257114 E−01
	$c2$	−0·164199 E+01	−0·441082 E+00	−0·433318 E−01	−0·316451 E−02	−0·760091 E+00	−0·496738 E+01	−0·396130 E+00	−0·400894 E+00	−0·408329 E+00	−0·525606 E−02
	$c3$	+0·478349 E+01	+0·358258 E+01	+0·318483 E+01	+0·470316 E+01	+0·704009 E+01	+0·153874 E+02	+0·150613 E+01	+0·197089 E+01	+0·300833 E+01	+0·157526 E+01
	m	−0·207315 E+00	−0·331202 E−01	−0·126178 E+00	−0·110135 E−02	−0·348161 E+00	−0·240813 E+01	−0·245402 E−01	−0·633544 E−01	−0·125199 E+00	−0·126499 E−02

Table VII. Dimensionless coefficients of spring-dashpot-mass model of Figures 11 and 13 for cylinder embedded in layer (Poisson's ratio $v = 1/3$ and embedment ratio $e/r_0 = 1$)

Ratio of Radius to Depth r_0/d	Contact ratio e_c/e		Vertical	Horizontal	Rocking	Coupling	Torsional
1/2	1·0	$k1$	− 0·203759 E + 02	− 0·124401 E + 02	− 0·125229 E + 02	− 0·618776 E + 01	− 0·139252 E + 02
		$k2$	+ 0·339543 E + 01	+ 0·286199 E + 01	− 0·583152 E + 00	+ 0·202777 E + 01	− 0·275441 E + 01
		$k3$	− 0·617014 E + 01	− 0·208541 E + 02	− 0·814822 E − 01	− 0·141784 E + 02	+ 0·178780 E + 01
		$k4$	+ 0·166202 E + 02	+ 0·794575 E + 01	+ 0·130945 E + 02	+ 0·337083 E + 01	+ 0·161164 E + 02
		$c1$	− 0·918456 E + 01	− 0·590158 E + 01	− 0·315268 E + 01	− 0·333135 E + 01	− 0·774712 E − 02
		$c2$	− 0·596381 E + 00	− 0·516028 E + 01	− 0·885823 E − 01	− 0·340080 E + 01	− 0·736101 E + 00
		$c3$	+ 0·131164 E + 02	+ 0·130103 E + 02	+ 0·322858 E + 01	+ 0·811310 E + 01	+ 0·858610 E + 01
		m	− 0·987169 E + 00	− 0·163126 E + 02	− 0·680666 E + 00	− 0·146553 E + 02	− 0·962102 E + 00
	0·5	$k1$	− 0·190169 E + 02	− 0·123585 E + 02	− 0·918010 E + 01	− 0·311508 E + 01	− 0·150459 E + 02
		$k2$	+ 0·102770 E + 02	+ 0·382788 E + 01	+ 0·934512 E + 00	+ 0·786487 E + 00	+ 0·149201 E + 01
		$k3$	− 0·256293 E + 02	− 0·116229 E + 02	− 0·466308 E + 01	− 0·869559 E + 01	− 0·230599 E + 01
		$k4$	+ 0·480379 E + 01	+ 0·697738 E + 01	+ 0·821627 E + 01	+ 0·184030 E + 01	+ 0·132374 E + 02
		$c1$	− 0·803919 E + 00	− 0·129978 E + 01	− 0·212247 E + 01	− 0·715314 E + 00	− 0·513171 E + 00
		$c2$	− 0·378972 E + 01	− 0·357027 E + 01	− 0·316747 E + 00	− 0·208337 E + 01	− 0·403901 E + 00
		$c3$	+ 0·131677 E + 02	+ 0·102413 E + 02	+ 0·266675 E + 01	+ 0·326137 E + 01	+ 0·511390 E + 01
		m	− 0·364874 E + 01	− 0·820645 E + 01	− 0·342125 E + 01	− 0·888905 E + 01	− 0·515523 E + 00
	0·0	$k1$	− 0·199866 E + 02	− 0·113528 E + 02	− 0·801960 E + 01	—	− 0·820959 E + 01
		$k2$	+ 0·324059 E + 01	+ 0·187819 E + 01	+ 0·103933 E + 01	—	+ 0·236828 E + 00
		$k3$	− 0·138239 E + 03	− 0·141228 E + 02	− 0·800817 E + 01	—	− 0·295213 E + 00
		$k4$	+ 0·151110 E + 02	+ 0·837372 E + 01	+ 0·584466 E + 01	—	+ 0·794727 E + 01
		$c1$	− 0·577181 E + 01	− 0·169786 E + 01	− 0·101867 E + 01	—	− 0·288545 E + 00
		$c2$	− 0·891247 E + 01	− 0·396633 E + 01	− 0·157192 E + 01	—	− 0·308176 E − 01
		$c3$	+ 0·151425 E + 02	+ 0·710633 E + 01	+ 0·313092 E + 01	—	+ 0·160082 E + 01
		m	− 0·485815 E + 02	− 0·142894 E + 02	− 0·217586 E + 01	—	− 0·372596 E − 01
1/3	1·0	$k1$	− 0·215677 E + 02	− 0·800686 E + 01	− 0·112339 E + 02	− 0·531331 E + 01	− 0·158881 E + 02
		$k2$	+ 0·995664 E + 01	+ 0·248098 E + 01	+ 0·271244 E + 01	+ 0·128879 E + 01	− 0·216892 E + 01
		$k3$	− 0·299529 E + 02	− 0·530555 E + 01	− 0·112792 E + 02	− 0·117090 E + 02	+ 0·122884 E + 01
		$k4$	+ 0·122789 E + 01	+ 0·460883 E + 01	+ 0·830774 E + 01	+ 0·314281 E + 01	+ 0·175253 E + 02
		$c1$	− 0·214856 E + 01	− 0·638370 E − 01	− 0·185381 E + 01	− 0·345899 E + 01	− 0·770582 E + 00
		$c2$	− 0·703468 E + 01	− 0·234186 E + 01	− 0·147482 E + 01	− 0·442673 E + 01	− 0·114118 E + 01
		$c3$	+ 0·195563 E + 02	+ 0·101919 E + 02	+ 0·461482 E + 01	+ 0·913903 E + 01	+ 0·899118 E + 01
		m	− 0·476605 E + 01	− 0·598035 E + 01	− 0·101760 E + 02	− 0·222249 E + 02	− 0·244900 E + 01
	0·5	$k1$	− 0·263609 E + 02	− 0·105510 E + 02	− 0·812675 E + 01	− 0·258694 E + 01	− 0·164865 E + 02
		$k2$	+ 0·106994 E + 02	+ 0·323771 E + 01	+ 0·327590 E + 01	+ 0·487010 E + 00	+ 0·162631 E + 01
		$k3$	− 0·415582 E + 02	− 0·101866 E + 02	− 0·183711 E + 02	− 0·708382 E + 01	− 0·359665 E + 01
		$k4$	+ 0·391023 E + 00	+ 0·579774 E + 01	+ 0·434718 E + 01	+ 0·155304 E + 01	+ 0·138158 E + 02
		$c1$	− 0·734715 E − 02	− 0·691681 E − 01	− 0·831614 E + 00	− 0·752538 E + 00	− 0·786309 E + 00
		$c2$	− 0·101472 E + 02	− 0·475156 E + 01	− 0·272228 E + 01	− 0·265221 E + 01	− 0·129218 E + 01
		$c3$	+ 0·195330 E + 02	+ 0·114226 E + 02	+ 0·507228 E + 01	+ 0·383021 E + 01	+ 0·600218 E + 01
		m	− 0·674277 E + 01	− 0·148975 E + 02	− 0·147137 E + 02	− 0·128622 E + 02	− 0·159889 E + 01
	0·0	$k1$	− 0·147108 E + 02	− 0·922525 E + 01	− 0·736535 E + 01	—	− 0·790274 E + 01
		$k2$	+ 0·600489 E + 01	+ 0·187933 E + 01	− 0·907967 E + 00	—	+ 0·176502 E − 01
		$k3$	− 0·355109 E + 02	− 0·788239 E + 01	− 0·157724 E + 03	—	− 0·179897 E − 01
		$k4$	+ 0·527313 E + 01	+ 0·637232 E + 01	+ 0·684877 E + 01	—	+ 0·788488 E + 01
		$c1$	− 0·203850 E + 01	− 0·425306 E − 01	− 0·168579 E + 01	—	− 0·128670 E + 00
		$c2$	− 0·830045 E + 01	− 0·368700 E + 01	− 0·114538 E + 02	—	− 0·263292 E − 03
		$c3$	+ 0·145304 E + 02	+ 0·682700 E + 01	+ 0·130128 E + 02	—	+ 0·157125 E + 01
		m	− 0·200705 E + 02	− 0·139626 E + 02	− 0·920928 E + 02	—	− 0·331649 E − 03

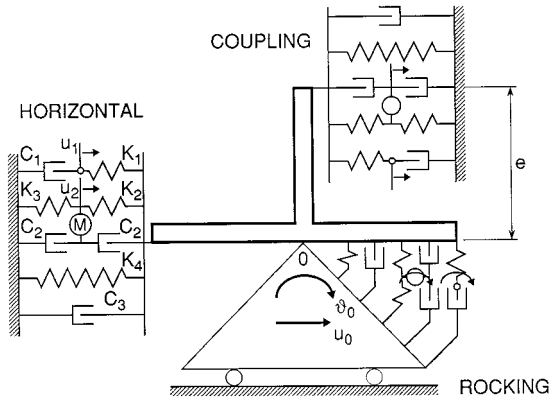

Figure 13. Spring-dashpot-mass model for cylinder embedded in layer with coupling of horizontal and rocking motions

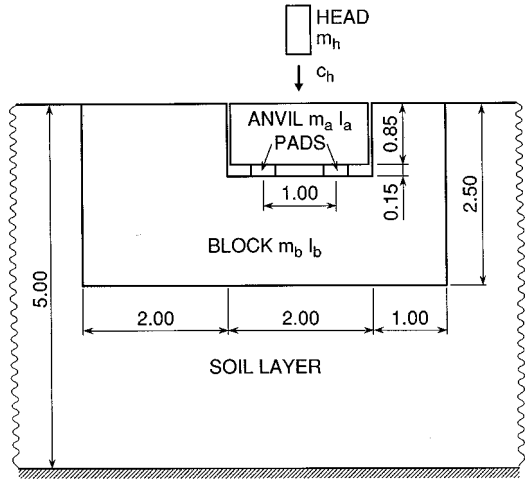

Figure 14. Hammer foundation with inertial block embedded in soil layer on rigid rock (all dimensions in meters)

The coefficients of the spring-dashpot-mass models of a cylinder embedded in a layer fixed at its base follow for the vertical, horizontal and rocking motions and for the coupling term $r_0/d = 1$ and $e_c/e = 1$ from Table VII (Figure 15). In the linear case, that is without uplift, there are 4×2 degrees of freedom for the spring-dashpot-mass models of the soil and 2×3 rigid-body degrees of freedom for the anvil and the block. The dynamic system's response—a free vibration—is triggered by the initial velocity of the anvil in the vertical direction.

The coupled dynamic model of Figure 15 can straightforwardly be analysed with a structural dynamics program permitting local non-linearities to occur. As expected, the uplift of the anvil increases significantly the vertical displacement w_a of the anvil when compared with the result of a linear analysis (Figure 16).

7. SOIL PRESSURE ON VERTICAL WALL FOR SEISMIC EXCITATION

Spring-dashpot-mass models with frequency-independent coefficients and with a few internal degrees of freedom can be constructed for practical use in many other cases. As an example, a spring-dashpot-mass

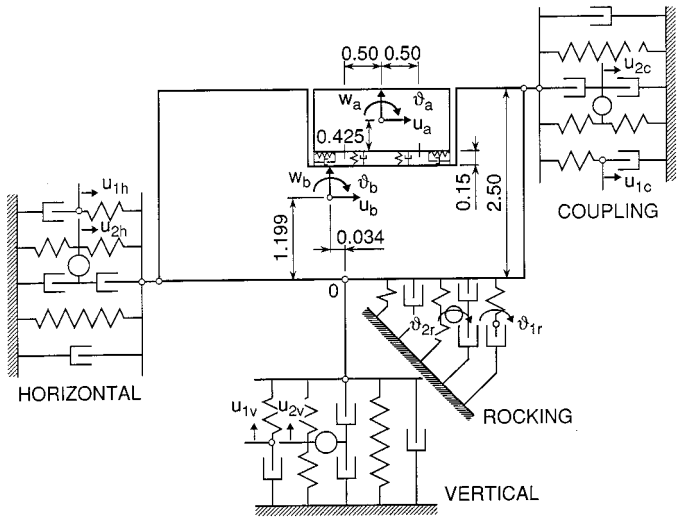

Figure 15. Dynamic model of hammer foundation with spring-dashpot-mass model

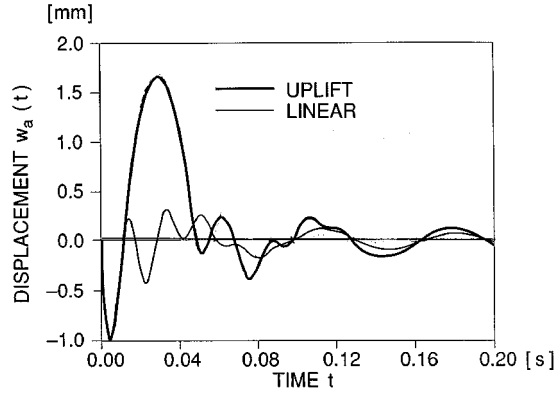

Figure 16. Vertical displacement of centre of anvil

model to calculate the dynamic pressure on a vertical rigid wall retaining a semi-infinite soil layer on rigid rock caused by a horizontal earthquake (Figure 17) is addressed.[16]

The model to perform a seismic analysis directly in the time domain is shown in Figure 18. On the mass m with its degree of freedom u_0 acts the load $-m\ddot{u}^g(t)$ with the known seismic acceleration time history of the rock's interface $\ddot{u}^g(t)$. The spring-dashpot part has three internal degrees of freedom u_1, u_2, u_3. The coefficients of the mass, the 4 springs and 4 dashpots are equal to

$$m = 0{\cdot}543 \frac{2}{\sqrt{(1-\nu)(2-\nu)}} \rho h^2 \tag{8a}$$

$$K_1 = -0{\cdot}682\omega_1^2 m \tag{8b}$$

$$K_2 = -0{\cdot}318\omega_1^2 m \tag{8c}$$

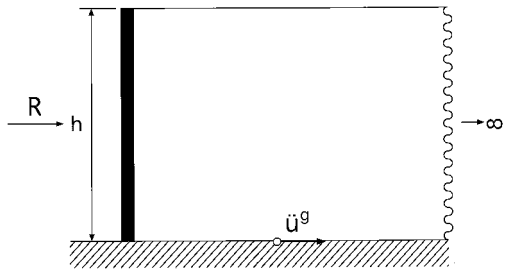

Figure 17. Vertical rigid wall retaining a semi-infinite soil layer on rigid rock with prescribed horizontal seismic motion at its base

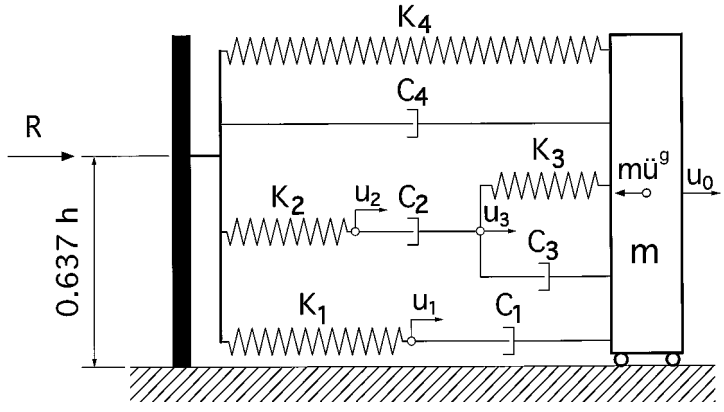

Figure 18. Spring-dashpot-mass model to calculate resultant pressure on vertical rigid wall

$$K_3 = 0{\cdot}273\omega_1^2 m \tag{8d}$$

$$K_4 = 2\omega_1^2 m \tag{8e}$$

$$C_1 = -0{\cdot}658\omega_1 m \tag{8f}$$

$$C_2 = -0{\cdot}344\omega_1 m \tag{8g}$$

$$C_3 = 0{\cdot}232\omega_1 m \tag{8h}$$

$$C_4 = \omega_1 m \tag{8i}$$

with Poisson's ratio v, mass density ρ and layer thickness d. ω_1 is the circular natural frequency of the layer ($\pi c_s/(2d)$) with shear-wave velocity $c_s = \sqrt{G/\rho}$ and shear modulus G. The resultant dynamic soil pressure R acts at a height $= 0{\cdot}637h$ (Figure 18). These coefficients apply for a soil layer without material damping. As for spring-dashpot-mass models of the dynamic-stiffness coefficients, material damping can be introduced directly into the algorithm.[12,13] Excellent agreement of the results with those of the approximate but accurate solution of Reference 17 arises.

8. CONCLUSIONS

A foundation can be accurately represented for all motions using a spring-dashpot-mass model with frequency-independent coefficients and a few internal degrees of freedom. The data to construct these models

are listed in tables for a rigid disk on the surface of a homogeneous half-space and a homogeneous layer fixed at its base and for a rigid cylinder embedded in a homogeneous half-space and a homogeneous layer fixed at its base, varying the parameters extensively. The foundation is thus modelled in the same way as the structure. The spring-dashpot-mass model of the foundation can be coupled with the dynamic model of the structure, permitting an unbounded soil–structure interaction analysis to be performed with a standard structural dynamics program. As an example, the non-linear analysis of a hammer foundation is presented. A spring-dashpot-mass model to determine the resultant dynamic soil pressure acting on a rigid vertical wall retaining a semi-infinite soil layer resting on rigid rock for horizontal earthquake is also specified.

REFERENCES

1. G. Ehlers, 'The effect of soil flexibility on vibrating systems', *Beton Eisen* **41**, 197–203 (1942) (in German).
2. A. S. Veletsos and V. V. D. Nair, 'Torsional vibration of viscoelastic foundations', *J. Geotech. Engng. Div. ASCE* **100**, 225–246 (1974).
3. J. W. Meek and A. S. Veletsos, 'Simple models for foundations in lateral and rocking motion', *Proc. 5th World Conf. on Earthquake Engineering*, Vol. 2, Rome, 1974, 2610–2613.
4. A. S. Veletsos and V. V. D. Nair, 'Response of torsionally excited foundations', *J. Geotech. Engng. Div. ASCE* **100**, 476–482 (1974).
5. J. W. Meek and J. P. Wolf, 'Cone models for homogeneous soil', *J. Geotech. Engng ASCE* **118**, 667–685 (1992).
6. J. W. Meek and J. P. Wolf, 'Cone models for nearly incompressible soil', *Earthquake Engng Struct. Dyn.* **22**, 649–663 (1993).
7. R. V. Whitman, 'Soil-platform interaction', *Proc. Conf. on the Behavior of Offshore Structures*, Vol. 1, Norwegian Geotechnical Institute, Oslo, 1976, pp. 817–829.
8. F. E. Richart, J. R. Hall and R. D. Woods, *Vibrations of Soils and Foundations*, Prentice-Hall, Englewood Cliffs, NJ, 1970.
9. J. P. Wolf and D. R. Somaini, 'Approximate dynamic model of embedded foundation in time domain', *Earthquake Engng. Struct. Dyn.* **14**, 683–703 (1986).
10. J. P. Wolf, 'Consistent lumped-parameter models for unbounded soil: physical representation', *Earthquake Engng Struct. Dyn.* **20**, 11–32 (1991).
11. J. P. Wolf and A. Paronesso, 'Lumped-parameter model for a rigid cylindrical foundation embedded in a soil layer on rigid rock', *Earthquake Engng Struct. Dyn.* **21**, 1021–1038 (1992).
12. J. W. Meek and J. P. Wolf, 'Material damping for lumped-parameter models of foundations', *Earthquake Engng Struct. Dyn.* **23**, 349–362 (1994).
13. J. P. Wolf, *Foundation Vibration Analysis Using Simple Physical Models*, Prentice-Hall, Englewood Cliffs, NJ, 1994.
14. E. Kausel, Personal communication (1990).
15. A. S. Veletsos and B. Verbic, Basic response functions of viscoelastic foundations, *Earthquake Engng Struct. Dyn.* **2**, 87–102 (1973).
16. J. P. Wolf, 'Discussion on a paper by A. S. Veletsos and A. H. Younan', *Earthquake Engng Struct. Dyn.* **24**, 1287–1291 (1995).
17. A. S. Veletsos and A. H. Younan, 'Dynamic soil pressure on rigid vertical walls', *Earthquake Engng Struct. Dyn.* **23**, 275–301 (1994).

